NICE - Neutron Induced Charged particle Emission

K. Al-Khasawneh[1], E. Borris[1], B. Brückner[1], K. Eberhardt[3], P. Erbacher[1], S. Fiebiger[1], R. Gernhäuser[2], K. Göbel[1], T. Heftrich[1],T. Kisselbach[1], D. Kurtulgil[1], C. Langer[1], M. Reich[1], R. Reifarth[1], D. Renisch[3,4], B. Thomas[1], M. Volknandt[1], and M. Weigand[1].

[1] Goethe University Frankfurt, Germany
[2] Technical University Munich, Germany
[3] Johannes Gutenberg University Mainz, Germany
[4] HIM Helmholtz-Institut Mainz, Germany

E-mail: kafa.khasawneh@gmail.com

November 2019

Abstract. A new detector setup (NICE-detector) based on an organic plastic scintillator is presented. It will be used during experiments measuring neutron-induced reactions with a charged particle in the exit channel. The proposed design was tested at the Goethe University Frankfurt. One of the test cases was the capture cross-section of ^{209}Bi at different astrophysically important energies, including thermal capture cross-section and resonance integral. This research presents the performance of the detector setup, as well as preliminary results for the calculated cross-sections. The preliminary results demonstrate that the newly developed NICE-detector can be used to determine capture cross-sections with sufficient accuracy, and might be adopted in the future as an alternative for charged particle measurements in different nuclear and astrophysical applications.

1. Introduction

In the field of nuclear astrophysics, the understanding of nucleosynthesis via neutron-induced reactions is essential to answer fundamental questions. Therefore, the corresponding cross-section values need to be investigated at stellar conditions. One example of neutron-induced reactions that contribute to stellar nucleosynthesis are reactions with charged particles in the exit channel (n, z). For instance, to verify the s-process abundance of ^{36}S neutron capture cross-section of ^{33}S(n,α)^{30}Si and ^{36}Cl(n,p)^{36}S need to be investigated at stellar conditions [2]. Furthermore, the importance of this reaction also extends to medical and nuclear-material applications.

Despite this importance, experimental cross-section data for such reactions are still scarce or exist with some discrepancies. Measurement difficulties arise from the short-range of charged particles compared to gamma radiation, which hampers their detection.

This implies restricting target thickness to the range of micrometers; therefore, cross-section calculations will be performed under low reaction rate conditions.

In the last decades, gas-ionization chambers were widely used for charged particle measurement in neutron-induced reaction experiments [2, 3, 4, 5, 6]. The merit of this choice is their low sensitivity to neutron radiation, which makes the counting process possible in the existence of the neutron beam. In addition, ionization chambers have the advantage of high-efficiency measurement. Silicon detectors were also investigated for (n, z) cross-section measurement. Unlike ionization chambers, silicon detectors are very sensitive to neutron radiation and must be operated outside the neutron beam [7].

This study is devoted to developing and constructing a new detector setup, which we call the NICE-detector, with a significant sensitivity based on an organic plastic scintillator. This detector will be applied to experiments on neutron-induced reactions with charged particles in the exit channel.

2. NICE-detector design

In order to determine the physical requirements of the NICE-detector, one has to identify the sources of background radiation that exist in the measurement environment. In the field of astrophysics, two complementary methods were employed extensively as a means to study neutron-induced reactions, Neutron-Activation, and Time-of-Flight (ToF) techniques. The main sources of background radiation in such experiments are γ-flash and scattered neutrons. Therefore, an ideal detector should have high sensitivity to measure charged particles and low sensitivity for background radiation. In addition, a fast-timing detector is also required so it can recover very fast from the huge background count-rate, and achieve sufficient neutron-energy resolution when considering the ToF technique. Organic plastic scintillator is an excellent candidate, because it combines all the mentioned requirements. A thin layer in a range of micrometers is sufficient to stop charged particles with energies of several MeV and have low sensitivity to gamma radiation and neutrons. Moreover, plastic scintillators have a fast light response time of less than 3 ns.

The NICE-detector design is composed of a thin layer of plastic scintillator, coupled to two Photomultiplier Tubes (PMT) at one face of the scintillator foil and connected to readout electronics (See Figure 1). According to this flexible design, the scintillator thickness can be varied for each experiment. Ideally, the chosen thickness should not exceed the range of charged particles in the scintillator material. In this work, because we are concerned with measuring alpha particles of $\simeq 5.5$ MeV, the scintillator in use is a polyvinyltoluene (PVT) based material with the manufacturer's product code BC-408 [8], which has 26×7 cm^2 surface area and 0.1 mm thickness. The PMTs are type H2431-50 from Hamamatsu [9]. The NICE-detector schematic and final design are shown in Figure 1.

Author guidelines for IOP Publishing journals in LaTeX 2ε

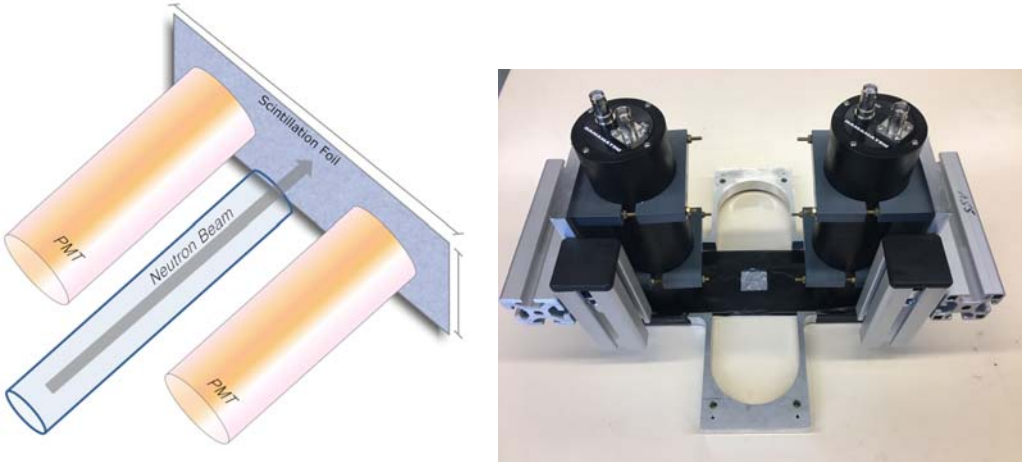

(a) (b)

Figure 1. (a) Schematic design represents the NICE-detector components and the expected neutron beam direction. (b) The NICE-detector and the PMTs supporting structure.

3. Detection efficiency of the NICE-detector

The Detection efficiency of NICE-detector was determined using an Americium radioactive source ^{241}Am (E_α= 5.5 MeV, I_α= 100%). A point source of activity 1.17 kBq was placed at the center and in close contact with the scintillation surface to avoid any measurable energy loss in the air.

Figure 2 shows the pulse height distribution of both PMTs as a function of channel number (relative light output). Due to the considerable distance between the interaction position and the PMTs centers (= 6.5 cm), light intensity measured by each PMT is relatively low; accordingly, the signal level is very low and overlaps with the electronic noise signals level. To distinguish between real scintillation pulse signals and electronic noise signals, we adopt a *Time-coincidence* technique using both PMTs (coincidence window = 50 ns). The real scintillation pulse from the specific physical event (*e.g* alpha) is detected by both PMTs nearly at the same time, while noise and background signals are mostly not correlated. The feasibility of this technique is illustrated in Figure 2 (b), which shows the pulse height distribution for the alpha peak after applying the time coincidence technique, where the noise and background levels are significantly reduced. The total detection efficiency was calculated from the total number of counts under the alpha-peak and was found to be $\varepsilon_{\alpha=5.5MeV}$ =(46.3 ± 0.4)%.

4. Measurement of the ^{209}Bi(n,γ)^{210}Bi cross-section using NICE-detector

The first practical test of the NICE-detector aimed to determine the ^{209}Bi capture cross-section. Accurate data of the ^{209}Bi(n,γ)^{210}Bi cross-section are necessary to explain the

Author guidelines for IOP Publishing journals in LaTeX 2ε

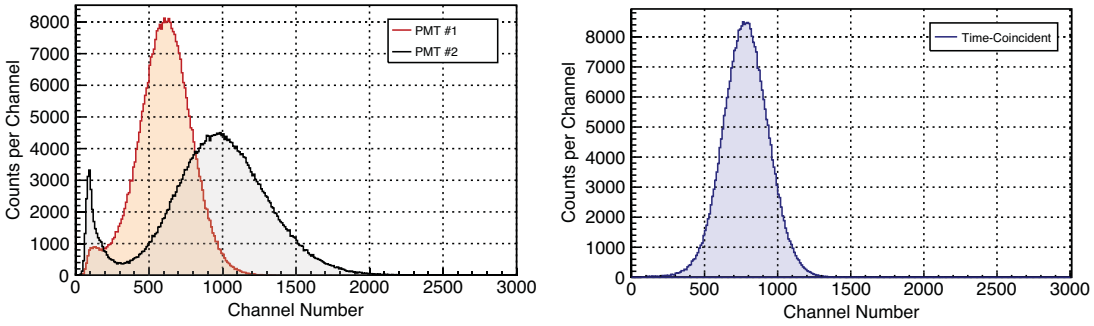

(a) (b)

Figure 2. (a) Pulse height distribution of ^{241}Am source obtained via PMT1 and PMT2. The different peak position is due to the different total gain. (b) Pulse height distribution after applying time-coincidence condition.

elemental abundances near the s-process termination point. Furthermore, capture cross-section values have become an essential matter after considering Pb-Bi as a coolant material in fast reactors and as a target material in Accelerator-Driven Systems (ADS).

According to the s-process scenario, ^{209}Bi is the last stable (or long-lived, $t_{1/2} \simeq 10^{19}$ Y [10]) isotope; all isotopes beyond ^{209}Bi are unstable against α-decay. Figure 3 demonstrates the s-process near Bi; the neutron capture on ^{209}Bi leads to the production of ^{210}Bi either in its ground state ^{210g}Bi or in the long-lived state ^{209m}Bi (E = 271.3 keV). All nuclei produced in their ground state undergo β-decay ($t_{1/2}$ = 5.03 days) to feed the α-unstable ^{210}Po isotope, which terminates the s-process chain and recycles its flow back to ^{206}Pb by emission of 5.3 MeV alpha particles with a half-life of $\simeq$ 138 days. ^{210}Po with a relatively long half-life can capture another neutron and contribute to the production of ^{207}Pb. On the other hand, the long-lived isomer state ($t_{1/2} = 3.04 \times 10^6$ Y) can also capture a neutron and lead to the production of ^{211}Bi, which undergoes α-decay into ^{207}Ti.

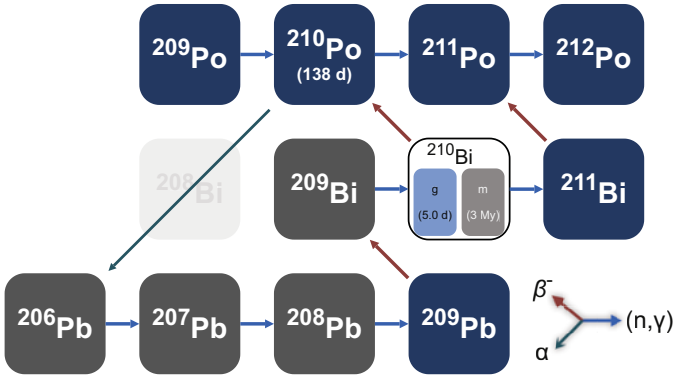

Figure 3. s-Process near the termination point.

Author guidelines for IOP Publishing journals in LaTeX 2ε

Table 1. Nuclear data for ^{197}Au and ^{45}Sc used in this work. Half-lives and emission probabilities are taken from the Brookhaven NNDC Database [24], while the neutron capture cross-section values are taken from ENDF [25].

Reaction	$t_{1/2}$ [d]	E_γ [keV]	I_0 [%]	σ_0 [barn]	I_0 [barn]
^{197}Au (n,γ)^{198}Au	2.69	411.8	95.62	98.7	1571
^{45}Sc (n,γ)^{46}Sc	83.79	889.3	99.99	27.2	12.06

Table 2. Masses and the number of atoms (N_0) for Bi-samples and neutron flux monitors.

Activation without Cd			Activation with Cd		
Sample	Mass [mg]	N_0 [$\times 10^{19}$ atoms]	Sample	Mass [mg]	N_0 [$\times 10^{19}$ atoms]
Bi-I	-	2.20 ± 0.55	Bi-I	-	2.18 ± 0.55
Au-1	1.1×10^{-2}	$(3.33 \pm 0.03)\times10^{-3}$	Au-3	1.0×10^{-2}	$(3.06 \pm 0.03)\times10^{-3}$
Au-2	1.1×10^{-2}	$(3.33 \pm 0.03)\times10^{-3}$	Au-4	1.1×10^{-2}	$(3.30 \pm 0.03)\times10^{-3}$
Sc-1	3.2	4.3 ± 0.1	Sc-3	2.7	3.62 ± 0.1
Sc-2	3.6	4.8 ± 0.1	Sc-4	4.2	5.63 ± 0.1

A number of experimental data of ^{209}Bi(n,γ)^{210g}Bi capture cross-section at different neutron energies were reported in previous studies, including thermal neutrons [11, 12, 13, 14], neutrons in the resonance region [15, 16, 17, 18], and neutrons with quasi-Maxwellian distribution at $kT = 30$ keV [19, 20, 21]. With an overview of this data and when compared to the evaluated values, one can see a considerable disagreement. Due to this discrepancy and for comparison purposes, new data are necessary.

In this work, we employed the NICE-detector to measure the ^{209}Bi(n,γ)^{210g}Bi capture cross-section at different astrophysical important energies, including effective thermal cross-section (σ_0), and resonance integral (I_0). The thermal activation took place in the research reactor TRIGA-Mark II at Johannes Gutenberg-University Mainz, Germany. The average neutron flux values at the irradiation position were determined using the *Two-Comparator Method* [22], while the Bi cross-section values were calculated based on *Cadmium-Ratio Difference Method*.

4.1. Samples and flux monitors

In this work, we used two Bi-samples (Bi-I and Bi-II), each composed of a thin layer of high purity ^{209}Bi (99.97 %) sputtered on polyester backing of 0.1 mm thickness. The Bi-layer has a dimension of 1.56 cm^2 surface area and 5 ± 1.2 μm thickness [23]. Wires of Al-0.1%Au alloy, and natural foils of ^{45}Sc (0.1 mm thickness) were used to determine the thermal and epithermal component of neutron flux. The corresponding decay data for both reactions are listed in Table 1.

To take into account the neutron flux gradient, the sample was positioned in-

between two monitor sets. Detailed parameters of the samples and monitors for each activation are given in Table 2.

4.2. Activation

The samples and flux monitors were sealed with plastic pockets to protect them from any external contamination, then packed into high purity polyethylene vials. We performed two activations with and without Cd-filter, each for 20 min. The Cd-filter was used to reduce the thermal component of the neutron flux at the irradiation position.

The total number of activated nuclei at the end of the activation interval course was expressed using the Høgdahl convention [26] as

$$N_{activation} = N_0(\sigma_0\phi_{th} + I_0\phi_{epi}), \tag{1}$$

where N_0 is the initial number of sample atoms, ϕ_0 and ϕ_{epi} are the time integrated thermal and epithermal neutron flux (n/cm^2), respectively. σ_0 and I_0 are thermal cross-section and resonance integral, respectively.

4.3. Calculations of ϕ_{th} and ϕ_{epi}

Induced activities for flux monitors were measured using HPGe-detector. The total number of activated nuclei ($N_{activation}$) is described as [27]

$$N_{activation} = \frac{C_\gamma}{\epsilon_\gamma I_\gamma k} \quad \frac{\lambda_\gamma t_a}{1 - e^{-\lambda t_a}} \quad \frac{1}{e^{-\lambda_\gamma t_w}} \quad \frac{1}{1 - e^{-\lambda_\gamma t_m}}, \tag{2}$$

where C_γ is the number of gamma counts in a particular gamma-line, ϵ_γ is the detector efficiency, λ_γ is the decay constant of the respective product nucleus, I_γ is the relative emission probability for a particular gamma energy, k is the dead-time correction factor, and determined from the ratio of real-to-live time, t_a, t_w, t_m are the activation, waiting and measurement times, respectively.

With the assumption that both flux monitors were exposed to the same neutron flux during the activation time course, ϕ_{th} and ϕ_{epi} can be calculated as follows

$$\phi_{th} = \frac{[\frac{^{198}{}_{Au}N}{^{197}{}_{Au}N}]I_0^{Sc} - [\frac{^{47}{}_{Sc}N}{^{46}{}_{Sc}N}]I_0^{Au}}{\sigma_0^{Au}I_0^{Sc} - \sigma_0^{Sc}I_0^{Au}}, \tag{3}$$

$$\phi_{epi} = \frac{[\frac{^{198}{}_{Au}N}{^{197}{}_{Au}N}]\sigma_0^{Sc} - [\frac{^{47}{}_{Sc}N}{^{46}{}_{Sc}N}]\sigma_0^{Au}}{\sigma_0^{Sc}I_0^{Au} - \sigma_0^{Au}I_0^{Sc}}. \tag{4}$$

Table 3 gives the total number of activated nuclei, time integrated flux values, and the corresponding average flux values seen by Bi-sample for both activations. It also provides the statistical uncertainties determined from the total number of counts under the gamma-peak ($\Delta_{stat} = \sqrt{C_\gamma}$), while systematic uncertainties originated from the γ-efficiencies, decay intensities, half-lives and cross-section values.

Author guidelines for IOP Publishing journals in LaTeX 2ε

Table 3. $N_{activation}$ and the time integrated neutron fluxes.

Monitor	$N_{activation} \pm \Delta_{stat} \pm \Delta_{sys}$ [$\times 10^9$ atoms]	$\phi_{th} \pm \Delta_{stat} \pm \Delta_{sys}$ [$\times 10^{13}$ n/cm^2]	$\phi_{epi} \pm \Delta_{stat} \pm \Delta_{sys}$ [$\times 10^{13}$ n/cm^2]
Activation without Cd			
Au-1	3.520 ± 0.034 ± 0.004	59.3 ± 0.69 ± 1.95	3.00 ± 0.03 ± 0.09
Sc-1	706.54 ± 4.44 ± 0.72		
Au-2	3.145 ± 0.030 ± 0.003	54.9 ± 0.63 ± 1.63	2.56 ± 0.03 ± 0.08
Sc-2	734.91 ± 4.71 ± 0.75		
Average Flux		**57.1 ± 0.66 ± 1.79**	**2.78 ± 0.03 ± 0.09**
Activation with Cd			
Au-3	1.371 ± 0.015 ± 0.002	0.028 ± 0.0005 ± 0.001	2.85 ± 0.05 ± 0.11
Sc-3	12.71 ± 0.16 ± 0.01		
Au-4	1.381 ± 0.015 ± 0.002	0.036 ± 0.0005 ± 0.001	2.66 ± 0.04 ± 0.07
Sc-4	18.61 ± 0.20± 0.02		
Average Flux		**0.032 ± 0.0005 ± 0.001**	**2.76 ± 0.04 ± 0.09**

4.4. Calculations of σ_0 and I_0

The induced activities of Bi-samples were measured using the NICE-detector. Since the ^{210}Po half-life is long relative to that for ^{210}Bi, waiting time in the range of $\simeq$ 77 days was sufficient to reduce the ^{210}Bi activity (β^- activity) into negligible levels, and at the same time reach a measurable level of ^{210}Po activity. In order to investigate the alpha-peak decay behaviour, we performed 35 consecutive measurements each for 24 hours. An example of a typical alpha peak obtained from one measurement is given in Figure 4.

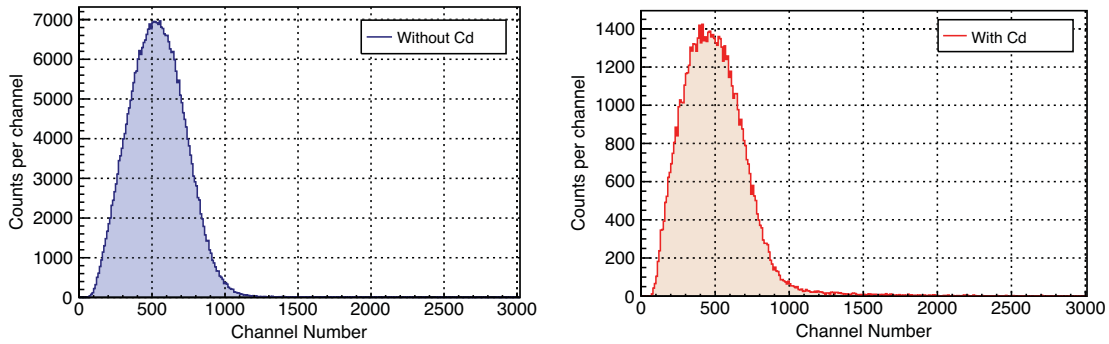

(a) (b)

Figure 4. Alpha peak obtained using the NICE-detector for the activated bismuth samples, both spectra obtained on day 77 after the activation and for 24 hours. (a) Activation without Cd-filter, (b) Activation with Cd-filter.

Author guidelines for IOP Publishing journals in LaTeX 2ε

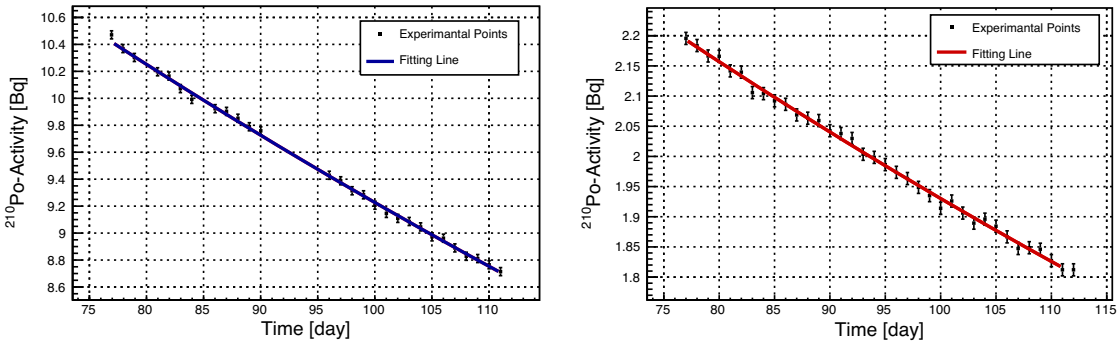

(a) (b)

Figure 5. ^{210}Po activity behaviour with time for the activated bismuth samples. (a) Activation without Cd-filter, (b) Activation with Cd-filter.

For each measurement, the ^{210}Po activity was deduced from the total number of counts under the alpha peak (C_α) as follows

$$A_{Po}(t) = \frac{C_\alpha}{\varepsilon_{\alpha=5.5MeV}\ t_m}, \tag{5}$$

where t is the time difference between the end of activation to the middle of the measurement time, $\varepsilon_{\alpha=5.5MeV}$ is the NICE-detector detection efficiency estimated in this work (Section 3), and t_m is the measurement time and equal to 24 hours.

The total number of activated nuclei in each Bi-sample was determined by fitting the ^{210}Po activity over 35 days using the function

$$A_{Po}(t) = \frac{N_{activation}\ \lambda_{Bi}\ \lambda_{Po}}{\lambda_{Po} - \lambda_{Bi}}(f_0 e^{-\lambda_{Bi}t} - f_1 e^{-\lambda_{Po}t}), \tag{6}$$

where λ_{Bi} and λ_{Po} are decay constants for ^{210}Bi and ^{210}Po, respectively, and f_0 and f_1 are corrections for the decay during activation. Experimental data of the ^{210}Po activity and the fitted curves are given in Figure 5 for both activations.

Based on the fitting results, the total number of activated nuclei are

$$N_{activation} = (25.98\ \pm\ 0.12_{stat}\ \pm\ 0.15_{sys})\ \times\ 10^7 \text{ atoms}, \tag{7}$$

$$N^{Cd}_{activation} = (5.59\ \pm\ 0.04_{stat}\ \pm\ 0.03_{sys})\ \times\ 10^7 \text{ atoms}. \tag{8}$$

Experimental values of the thermal cross-section and resonance integral were deduced from the measured total number of activated nuclei, and the time integrated thermal and epithermal neutron flux using the Cd-ratio difference method as follows:

$$\sigma_0 = \frac{[\frac{^{210}Bi_N}{^{209}Bi_N}]\phi^{cd}_{epi} - [\frac{^{210}Bi_N}{^{209}Bi_N}]^{cd}\phi_{epi}}{\phi_{th}\phi^{cd}_{epi} - \phi^{cd}_{th}\phi_{epi}}, \tag{9}$$

$$I_0 = \frac{[\frac{^{210}Bi_N}{^{209}Bi_N}]\phi^{cd}_{th} - [\frac{^{210}Bi_N}{^{209}Bi_N}]^{cd}\phi_{th}}{\phi^{cd}_{th}\phi_{epi} - \phi_{th}\phi^{cd}_{epi}}. \tag{10}$$

Author guidelines for IOP Publishing journals in LaTeX 2ε

Using the above approach, the preliminary results for the thermal cross-section and resonance integral values for ^{209}Bi(n,γ)^{210g}Bi were found to be

$$\sigma_0 = (16.16 \pm 0.47_{stat} \pm 5.81_{sys}) \text{ mb},$$
$$I_0 = (92.69 \pm 2.67_{stat} \pm 33.30_{sys}) \text{ mb}.$$

The relatively large systematical uncertainties arise from the 25% uncertainty in the sample thickness. We will soon improve this and derive a cross sections with less than 10% uncertainty.

According to our knowledge, this is the first experimental measurement of the resonance integral, while several measurements of the thermal cross-section have been reported in previous studies. Table 4 lists a number of experimental values obtained using the activation technique. Based on measuring the ^{210}Bi induced activity and by counting β-particles, Seren *et al.* [11] and Takiue and Ishikawae [13] reported two different values. Colmer and Littler [12] and Letourneau *et al.* [14] obtained the cross-section values by measuring ^{210}Po induced activity, and the low intensity gamma-ray coming from the de-excitation of ^{206}Pb (Letourneau *et al.*). The measured value in this work is in good agreement with Seren *et al.* and Letourneau *et al.*, but 21% lower than Colmer and Littler and 33% than Takiue and Ishikawa.

Table 4. An overview of the thermal capture cross-section data for ^{209}Bi(n,γ)^{210g}Bi reported in previous studies. Results for the thermal capture cross-section and resonance integral obtained in this work are also listed. Uncertainties are given in brackets.

Reference	Method, Detection	σ_g [mb]	I_0 [mb]	Ref.
Seren et al. (1947)	Activation, β	15 (2.0)		[11]
Colmer and Littler (1950)	Activation, α	20.5 (1.5)		[12]
Takiue and Ishikawa (1978)	Activation, β	24.2 (0.4)		[13]
Letourneau et al. (2006)	Activation, α	16.08 (1.8)		[14]
Letourneau et al. (2006)	Activation, γ	18.04 (0.9)		[14]
This work(NICE-detector)	Activation, α	16.16 (6.27)	92.96 (35.9)	

5. Conclusions

A new flexible detector design (NICE-detector) based on a thin layer of plastic scintillator connected to two PMTs was presented. This detector can be used as an alternative for charged particle measurement in neutron-induced reactions. In this work, the scintillator thickness was optimized according to the range of 5.5 MeV alpha particle in the scintillator material. The detection efficiency was measured using an ^{241}Am source and was found to be 46.3 ± 0.4 %. A first experimental test was performed to measure the capture cross-section of ^{209}Bi(n,γ)^{210g}Bi reaction. Preliminary results demonstrate that within the preliminary uncertainties, the thermal cross-section value obtained in this work agrees with the reported ones. In the future, uncertainties in the sample

thickness have to be reduced. For instance, sample thickness can be measured using Rutherford backscattering spectrometry (RBS).

Acknowledgment

Authors gratefully acknowledge the financial support by the DFG-project NICE (RE 3461/3-1). A special thanks are due to the staff of the TRIGA-reactor, Mainz.

References

[1] Käppeler F, Beer H and Wisshak K 1989 *Rep. Prog. Phys* **52** 945-1013.
[2] Schatz H, Jaag S, Linker G, Steininger R, Käppeler F, Koehler P, Graff S and Wiescher M 1995 *Phys. Rev. C* **51** 379–391.
[3] Popov Yu.P, Przytula M, Rumi R.F, Stempinski M and Frontayeva M 1972 *Nuclear Physics A* **188** 212-224.
[4] Wilkinson D.H. 1950 Ionization Chambers and Counters *New York: Cambridge Univ Press*
[5] Koehler P.E, Harvey J.A. and Hill N. W. 1995 *Nuclear Instruments and Methods in Physics Research A* **361** 270-276.
[6] Goeminne G, Wagemans C, Wagemans J, Serot O, Loiselet M and Gaelens M 2000 *Nuclear Physics A* **678** 11–23.
[7] Woods P.J, Lederer C, Käppeler F, Berthoumieux E, Chiaveri E, Colonna N, Davinson T, Guerrero C, Gunsing F, Heyse J, Lotay G, Massimi C, Mondelaers W, Reifarth R, Schillebeeckx P, Tagliente G, Wagemans C, Wallner A, Weiss C, and the nTOF Collaboration 2012 *CERN-INTC-2012-002*
[8] https://www.crystals.saint-gobain.com.
[9] https://www.hamamatsu.com/jp/en/product/alpha/P/3002/H2431-50/index.html.
[10] Marcillac P, Coron N, Dambier G and Leblanc J 2003 *Nature* **422** 876-878.
[11] Seren L, Friedlander H.N. and Turkel S.H. 1947 *Phys. Rev.* **72** 888–901.
[12] Colmer F.C.W and Little D. J 1950 *Proc. Phys. Soc. A* **63** 1175-1176.
[13] Takiue M and Ishikawa H 1978 *Nucl. Instr. Meth* **148** 157–161.
[14] Letourneau A, Fioni G, Marie F, Ridikas D and Mutti P 2006 *Ann. Nucl. Energy* **33** 377–384.
[15] Macklin R and Halperin J. 1976 *Phys. Rev. C* **14** 1389-1391.
[16] Domingo-Pardo C *et al.* 2006 *Phys. Rev. C.* **74** 025807.
[17] P. Mutti *et al.* 1988 *Proceedings of the International Symposium on Nuclear Astrophysics: Nuclei in the cosmos V* 204.
[18] Beer H, Voss F, and Winters R.R 1992 *ApJS.* **80** 403-424.
[19] Ratzel U, Arlandini C, Käppeler F, Couture A, Wiescher M, Reifarth R, Gallino R, Mengoni A and Travaglio C 2004 *Phys. Rev. C.* **70** 065803.
[20] Bisterzo S, Käppeler F, Gallino R, Heil M, Domingo-Pardo C, Vockenhuber C and Wallner A 2008 *International Conference on Nuclear Data for Science and Technology ND2007* 1333-1336.
[21] A. Shor *et al.* 2017 *Phys. Rev C* **96** 055805.
[22] Simonits A, de corte F and Hoste J 1976 *Journal of Radio analytical Chemistry* **31** 467-486.
[23] http://www.goodfellow.com/E/Bismuth-Foil.html.
[24] Brookhaven NNDC Database. http://www.nndc.bnl.gov/ensdf/. September 2019.
[25] M.B. Chadwick *et al.* 2011 *Nuclear Data for Science and Technology:ENDFB-VII.1 Nuclear Data Sheet,ENDFB-VII.1 Nuclear Data Sheet.* **112**.
[26] Høgdahl OT 1965 Radiochemical methods of analysis. IAEA, Vienna.
[27] Beer H and Käppeler F 1980 *Phys. Rev. C* **21** 534-544.